# Volumetric Stimulated Raman Scattering Imaging of Cleared Tissues towards Three-dimensional Chemical Histopathology

**Junjie Li,[1] Peng Lin,[1] Yuying Tan,[2] AND Ji-Xin Cheng[1,2,3,*]**

[1]*Department of Electrical and Computer Engineering, Boston University, 8 St. Mary's St, Boston, MA 02215, USA*
[2]*Department of Biomedical Engineering, Boston University, 44 Cummington Mall, Boston, MA 02215, USA*
[3]*Photonics Center, Boston University, 8 St. Mary's St, Boston, MA 02215, USA*
[*] *jxcheng@bu.edu*

**Abstract:** Thin tissue slice based histology has been used as a gold standard for disease diagnosis since over a hundred years ago. However, histopathological evaluation on two-dimensional slides suffers from large variations due to limited sampling. To improve the diagnostic accuracy, three-dimensional histology is performed through serial sectioning, staining, imaging and reconstruction of individual slices, which is highly time-consuming and labor intensive. We developed a volumetric stimulated Raman scattering (SRS) imaging method, which provides histology-like information within 30 min in 3D context without the need for staining. We improved the imaging depth of SRS microscopy by a content-reserving tissue clearing method. Using a small molecule clearing agent, formamide, we achieved an imaging depth of ~500 μm in highly scattered tissues, including brain, kidney, liver and lung. Through a two-color SRS imaging scheme, we obtained histology-like images in cleared brain tissue slices. Our method has the potential for 3D tissue histopathology to improve the accuracy of histopathological examination.

© 2018 Optical Society of America under the terms of the OSA Open Access Publishing Agreement

## 1. Introduction

Pathological examination has been a gold standard for disease diagnosis and prognosis. Conventional pathology is mostly performed on ultra-thin (4 to 6 μm) tissue slices stained with dyes, such as haematoxylin and eosin (H&E), to enhance structural and intracellular contrast. This microscopic examination on two-dimensional slices provides structural information with single-cell resolution. However, it lacks organizational information of important diagnostic features in three-dimensional context. The limited sampling from a bulk of tissues largely increases the inter- and intra-observer variability [1], reducing the reproducibility and accuracy of conventional pathology.

Considering these inherent drawbacks of two-dimensional pathology, there has been an increasing demand for three-dimensional histopathology [2]. One straightforward way to obtain three-dimensional pathology is to perform serial-sectioning, staining, imaging and reconstruction. This method is inevitably time-consuming, labor-intensive and destructive to the samples, and thus is not widely adopted in clinical use. To overcome these limitations, other imaging methods are being developed to replace staining-based histology. Optical coherence tomography (OCT) is a microscopic imaging modality with millimeter level penetration depth, yet without chemical selectivity or sufficient resolution (~ 10 μm) for identifying subcellular features [3, 4]. Numerous efforts have been devoted to developing infrared (IR) spectroscopic imaging toward chemical histopathology in the past decade [5-8]. However, this method suffers from relatively low resolution (>2 μm) and limited penetration depth (~30 μm). Although attenuated total reflection IR improves the resolution down to submicron scale, it is only feasible for surface imaging (penetration depth 1-3 μm) [9].

Recent advances in optical imaging techniques have highlighted other possibilities for histopathology. By taking advantage of the strong absorption of ultraviolet (UV) light (266 nm) by intrinsic molecules, such as DNA and RNA, Wong et al. achieved histology-like imaging of human breast cancer tissues using photoacoustic microscopy with excellent lateral resolution (~330 nm) [10]. Levenson and colleagues developed a microscope with ultraviolet surface excitation (MUSE) rapid slide-free histology [11]. Glaser et al. deployed light-sheet microscopy for slide-free pathology of clinical specimens with ~200 μm imaging depth [12]. Yet, these methods either suffers from a poor axial resolution (~48 μm) in the case of photoacoustic microscopy or requires staining with dyes where the imaging depth is ultimately limited by the penetration of dyes.

With intrinsic sectioning capability, nonlinear optical microscopy opens a new window for label-free histopathology. Balu *et al.* demonstrated the use of multiphoton microscopy for rapid examination of human skin tissues [13, 14]. Sun and co-workers applied second- and third-harmonic generation (S/THG) microscopies for virtual biopsy of human skin with a penetration depth of ~300 μm. Combination of Coherent anti-Stokes Raman Scattering (CARS), Two-Photon Excitation Fluorescence (TPEF), and SHG/THG microscopies produces H&E staining-like histology images, as demonstrated for tissue optical biopsy by the Popp group [15, 16] and the Boppart group [17].

Stimulated Raman scattering (SRS) microscopy, as a vibrational chemical imaging modality, provides label-free features with submicron resolution and chemical selectivity [18]. These characteristics of SRS microscopy fulfills the needs for histological imaging. Application of SRS microscopy for histopathology has been recognized and extensively studied in brain tumor detection [19-21]. However, due to limited penetration depth (< 50 μm) of SRS imaging in highly scattered tissues, translational use of SRS microscope is restricted to thin tissue sections [22]. Recently, several advances have been made to enable SRS-based volumetric chemical imaging. Utilizing Bessel beams for pump and Stokes, Chen *et al.* reported stimulated Raman projection tomography for volumetric chemical imaging with isotropic spatial resolution [23]. Through tissue clearing by urea, Wei *et al.* achieved volumetric SRS imaging by enhancing penetration depth [24]. However, the urea-based clearing requires days to weeks to complete, thus limiting its potential application in tissue histopathology and clinical diagnosis.

Here, we report a rapid clearing method that enables volumetric SRS imaging with a penetration depth of ~500 μm. By systematically comparing different clearing methods in composition and clearance time, we found that formamide-based clearing method is compatible with SRS imaging at C-H region with minimal background and provides a much faster clearing speed (~30 min) compared to other commonly used methods. We further demonstrate the versatility of this method in various organs, including brain, lung, liver, and kidney. Through two-color SRS imaging, we obtained histology-like images in three-dimensional context of brain tissues, which could potentially improve the diagnostic accuracy of histopathology by conventional 2D sectioning and staining method.

## 2. Experimental Methods

### *2.1 Stimulated Raman scattering (SRS) imaging setup*

Single-color and hyperspectral SRS imaging was performed on a lab-built SRS microscopy system. A femtosecond laser system (InSight DeepSee, Spectra-Physics) operating at 80 MHz was used as the excitation source. The center frequencies of the pump and Stokes beams were tuned to 798 nm and 1040 nm, respectively, to cover the C-H vibrational region. The Stokes beam was modulated by an acousto-optic modulator (1205-C, Isomet) at ~2.3 MHz. Hyperspectral SRS microscopy was achieved on a spectral focusing scheme as described previously [25]. Both femtosecond pulses were chirped using two 12.7 cm long SF57 glass rods. The temporal delay between pump and Stokes pulses was controlled by a motorized translational stage (T-LS28E, Zaber). The power for pump and Stokes beam was set as ~70

mW and ~400 mW (maximal power), respectively, before microscope. A 40X water-immersion objective (NA = 0.8, working distance = 3.3 mm, LUMPLFLN/40XW, Olympus) was used to focus the light on specimen and an oil condenser (NA = 1.4, U-AAC, Olympus) was used to collect the signal. Standard chemicals including Dimethyl Sulfoxide (DMSO) and oleic acid (Sigma) are used to calibrate the Raman shift to the temporal delay.

### *2.2 Two-color volumetric image acquisition and analysis*

To acquire volumetric images, an objective positioner (ND72Z2LAQ, Physik Intrumente) was installed to axially scan the laser foci in the sample with 20 ms settling time at each depth. The maximum display range is ~2 mm in axial direction. The step interval was set as 4 μm or 1 μm. With a pixel dwell time of 10 μs, the imaging speed is ~1.6 seconds per frame for an image of 400x400 pixel. To achieve two-color SRS images, a lab-built LabVIEW program was designed to control the delay sage moving back and forth between two temporal positions that correspond to 2850 $cm^{-1}$ and 2930 $cm^{-1}$ Raman shift. All images were processed and analyzed using ImageJ. The reconstructed 3D images were produced through the 3D plugin in ImageJ.

### *2.3 Raman spectra measurement*

Spontaneous Raman spectra of the clearing solutions were acquired on a confocal Raman microscope (LabRAM HR Evolution, HORIBA). A 532 nm continuous wave laser was used as the excitation light. A 600 lines/mm grating was selected. Spectra in the range from 300 to 3400 $cm^{-1}$ were collected with exposure time of 5 ~ 10 seconds. Raman spectra were processed in Origin software.

### *2.4 Mouse tissue collection*

Balb/c mice (Jackson Laboratory) at ~8 weeks old were used in this study for tissue clearance and imaging. Mice were anesthetized under ~3% isoflurane inhalation, followed by perfusion with phosphate buffered saline (PBS) and 10% formalin. Organs, including brain, liver, lung, and kidney, were harvested and placed in 10% formalin for overnight or longer time. All animal experiments were conducted following protocols approved by Boston University Institutional Animal Care & Use Committee (IACUC).

### *2.5 Tissue preparation and clearance*

Formalin-fixed tissues were sectioned into slices with 500 ~ 1000 μm thickness using a microtome. Tissue slices were placed in PBS buffer before clearance. Chemicals for tissue clearance, including formamide, sucrose, urea, glycerol, fructose, Triton X-100 and 1-Thioglycerol, were purchased from Sigma. Tissue clearing was performed following previously described procedures. For ScaleA2 method, tissue slices were immersed in solution composed of 4M Urea, 10% (w/v) glycerol, and 0.1% Triton X-100 for two days. For sucrose method, tissue slices were immersed in a series of sucrose solutions with increasing concentrations of sucrose at 15%, 30%, 45%, and 60% sucrose plus 2% Triton X-100 with 6 h equilibration time for each step. For ClearT method, tissue slices were immersed in 20%, 40%, 80%, and 95% formamide solutions with 5 min for each step and additional 15 min in 95% formamide solution. Same procedures were followed when the tissue slices were cleared with formamide solution with 5% Triton X-100. Before imaging, the cleared slices were mounted on glass coverslip with 1% (w/v) agarose gel to prevent sample movement during imaging. Another coverslip was covered on the top the slice.

## 3. Results

### *3.1 Comparison of different clearing methods*

Tissue clearance has been widely used in fluorescence microscopy for whole tissue imaging and various tissue clearing methods have been developed. Tissue clearing agents improve

**Table 1. Comparison of different clearing methods in composition and clearance time.**

| Method | Solutions | Time needed |
|---|---|---|
| ScaleA2 | 4M Urea, 10% (wt/vol) glycerol, 0.1% Triton X-100 | > 2 days |
| Sucrose | 15, 30, 45, 60% sucrose + 2% Triton X-100 | 4 days |
| ClearT | 20%, 40%, 80%, and 95% formamide solutions in PBS (v/v) | 30 min |

imaging depth largely by reducing light scattering through several steps, including removal of lipids and correction of refractive index mismatch. Based on the clearing agents, the established tissue clearing methods fells into three categories, organic solvent, aqueous solution and hydrogel [26]. Organic solvents dissolve most of the lipids and create a refractive index matching environment. Aqueous solutions match refractive index mainly through small molecule diffusion. Hydrogel embedding expand the tissue specimen by crosslinking followed by refractive index matching. As SRS microscopy produces strongest signal from the C-H vibrational region, which will used for histopathological imaging. To avoid the lipid and protein loss from harsh organic solvents and to minimize the background signal from hydrogel, we decide to use high refractive index aqueous solutions composed of small diffusive molecules.

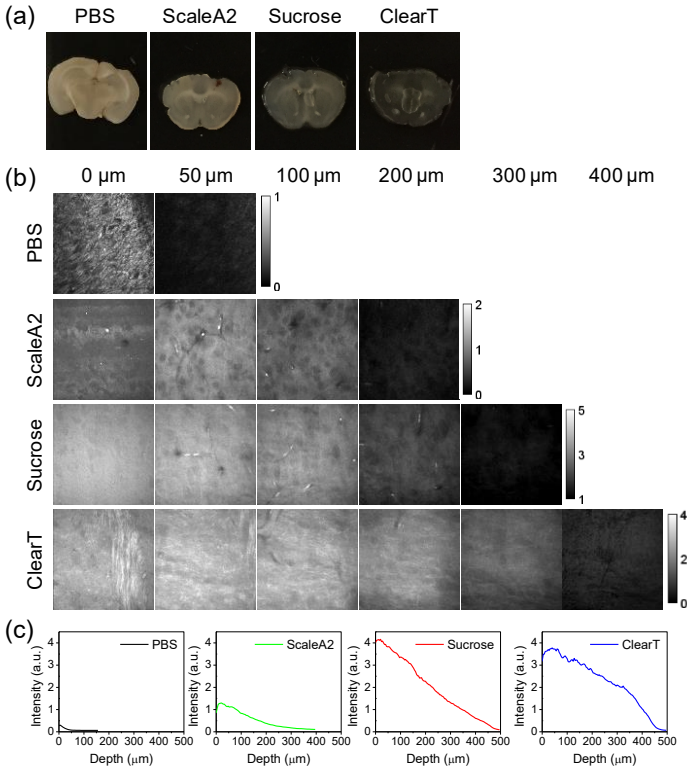


**Fig 1. Comparison of different clearing methods.** (a) Pictures of brains slices (~500 μm thick) cleared with different methods. (b) SRS images taken at 2930 $cm^{-1}$ from brain slices cleared by different methods at indicated depth. (c) Intensity profile over depth from the images shown in (b).

We chose to test a few commonly used and economically-favorable methods, including Sucrose [27], ScaleA2 [28], and ClearT [29]. To evaluate the performance of these methods, we sectioned brain tissue into 500 μm thick slices. The clearing solutions were prepared following previous reports. Brain slices with same thickness were placed into various clearing agents for indicated period. As shown in **Table 1**, brain slices were immersed in Scale A2 solution for 2 days, in sucrose solutions for 4 days, and in ClearT solution at serial concentration

gradient for only 30 min. After clearing, brain slices were placed together for visual comparison. As shown in **Fig. 1A**, compared to PBS immersion group (control), the other three slices all showed increased transparency, while ClearT group showed highest transparency. Then, SRS imaging at 2930 $cm^{-1}$ was performed to these brain slices. A piezo-stage was used to control the imaging depth with an interval of 4 µm. SRS signal diminishes quickly in tissue specimen without clearing as the depth increases and no discernible features can be distinguished at 50 µm depth (**Fig. 1B, Movie 1**). Imaging depth was improved to ~200 µm in ScaleA2 treated slices (**Fig. 1B, Movie 2**) and ~300 µm in sucrose treated slice (**Fig. 1B, Movie 3**). In contrast, recognizable contrast is observed at up to 400 µm depth in tissue slices immersed in ClearT solution (**Fig. 1B, Movie 4**). Compared to other groups, ClearT solution treated slice also show higher SRS intensity and slower signal decay with depth increases (**Fig. 1C**). These results suggest that ClearT is compatible with SRS imaging with shorter incubation time and deeper imaging depth in tissues.

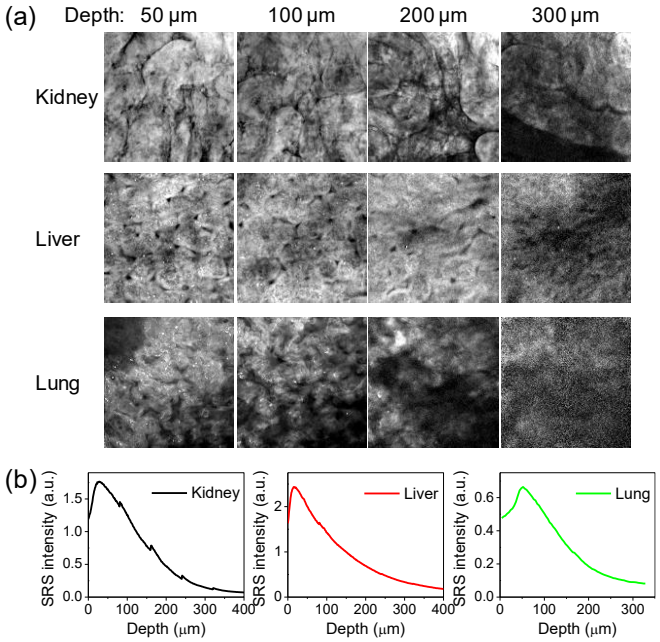


**Fig 2. Demonstration of tissue clearance in various organs.** (a) SRS images taken at 2930 $cm^{-1}$ from kidney, liver and lung tissue slices (~ 1 mm thick) at indicated depth. (b) Intensity profile over depth from the images in (a).

### *3.2 Versatility in various organs*

Besides brain tissues, we also tested the tissue clearing methods in various types of organs, including kidney, liver and lung. Formalin fixed tissues were cut into 1000 µm thick tissue slices and cleared using ClearT method. Tissue slices become visually transparent in ~30 min followed by SRS imaging at various depth. Tissue structure and organization are recognizable at depth of ~300 µm in kidney (**Fig. 2A, Movie 5**), liver (**Fig. 2A, Movie 6**) and lung tissue slice (**Fig. 2A, Movie 7**). Quantitative analysis of the SRS signal shows faster signal decay in kidney, liver and lung tissue slices (**Fig. 2B**), compared to brain slices, which is likely due to light absorption by pigments, such as hemoglobin, in these tissues. With decoloring, the imaging depth will be further improved.

### *3.3 Spectral measurement of clearing agents*

To understand the SRS signal source in the cleared tissue slices, we analyzed the background signal from the clearing agents through hyperspectral SRS imaging. Compared to PBS, all the clearing solution showed higher SRS signal at 2850 $cm^{-1}$ and 2930 $cm^{-1}$, with strongest signal

from sucrose solution (**Fig. 3A**). SRS spectra at the C-H vibrational region from 2800 ~ 3050 $cm^{-1}$ clearly showed higher signal from sucrose and ClearT solution and relatively lower signal from ScaleA2 solution (**Fig. 3B**). However, sucrose solution shows much broader spectrum in this region than ClearT solution. ClearT solution has a relatively narrow spectrum with the peak position at ~2890 $cm^{-1}$, suggesting a possible way to minimize background signal by selecting off-peak Raman shift positions. The SRS spectral measurements were confirmed by Raman spectra measured by spontaneous Raman spectroscopy (**Fig. 3C**). Considering the relative low penetration depth from ScaleA2 solution and strong background signal from sucrose solution, ClearT method appears to be the best one for SRS imaging based tissue clearing.

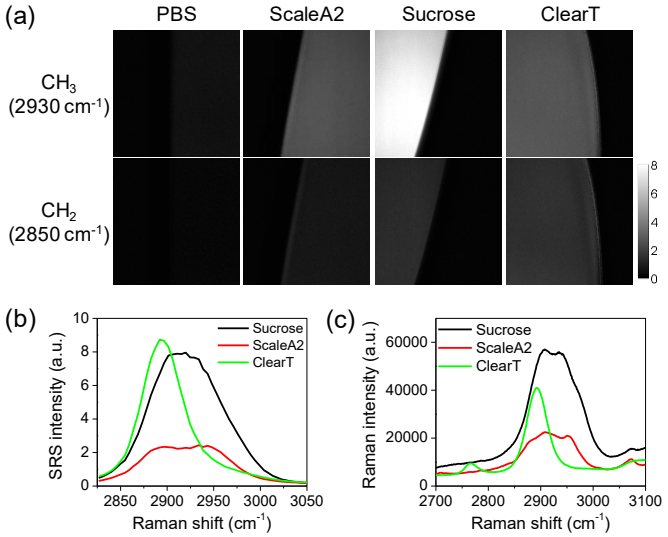


**Fig 3. Spectroscopic analysis of different clearing solutions.** (a) SRS images of different clearing solutions at 2930 $cm^{-1}$ and 2850 $cm^{-1}$. (b) SRS spectra of clearing solutions in the region from 2800 $cm^{-1}$ to 3050 $cm^{-1}$. (c) Raman spectra taken by spontaneous Raman spectroscopy with 532 nm as excitation light.

### *3.4 Optimizing the protocol to increase imaging depth*

To further improve the imaging depth, we optimized the protocol by adding detergent in the clearing solution. Detergent partially removes the lipids, which cause the most significant scattering in tissues, but not like organic solvents, detergents remain the cell morphological integrity. As for histopathology, tissue structural organization, cell morphology and nucleus size are important features in pathological examination. Using detergents will not affect the structural and morphological information of tissues. Using 1000 μm thick brain slices, we tested tissue clearing with ClearT solution and ClearT with additional 5% Triton X-100. Similar like above mentioned, without detergent SRS images with clear contrast can be achieved with up to ~ 400-μm depth (**Fig. 4A, Movie 8**). However, with 5% Triton X-100, the imaging depth is further enhanced to ~500 μm with resolvable image contrast (**Fig. 4A, Movie 9**). With this imaging depth, two cortex layers in the axial direction can be clearly revealed (**Fig. 4B, Movie 10**). Furthermore, use of detergent also enhance the signal intensity compared to ClearT alone (**Fig. 4B**). Nevertheless, it does not significantly increase the background signal, as indicated by the Raman spectral measurement of the clearing solutions (**Fig. 4C**).

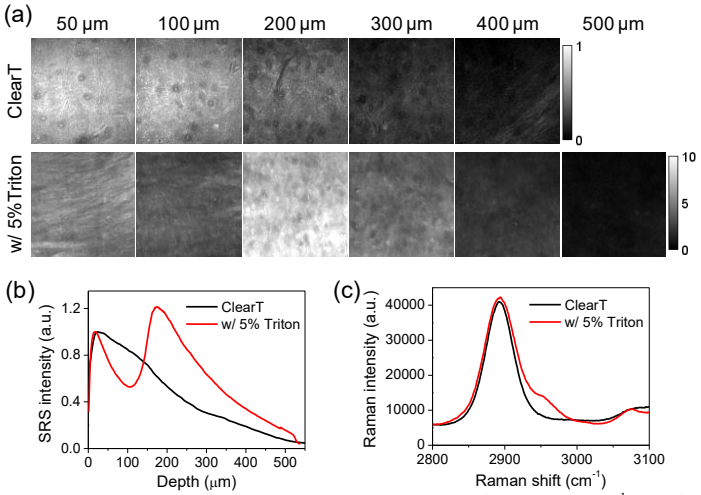


**Fig 4. Improvement of imaging depth with detergent.** (a) SRS images taken at 2930 $cm^{-1}$ from brain slices (~1 mm thick) cleared by ClearT solution with or without 5% Triton X-100 at indicated depth. (b) Intensity profile over depth from the images shown in (a). (c) Raman spectra of ClearT solution with or without 5% Triton X-100.

### *3.5 3D histopathological imaging of cleared tissues by two-color SRS*

To generate histology-like images, we take advantage of chemical selectivity of SRS microscopy. Hyperspectral SRS microscopy can readily separate cellular compartments, such as nucleus and cytoplasm [30]. However, hyperspectral SRS microscopy takes long time to scan the spectrum. To create the contrast needed for histopathology, we used two-color SRS microscopy at 2850 $cm^{-1}$ and 2930 $cm^{-1}$, which originates from $CH_2$ and $CH_3$ vibration, respectively.

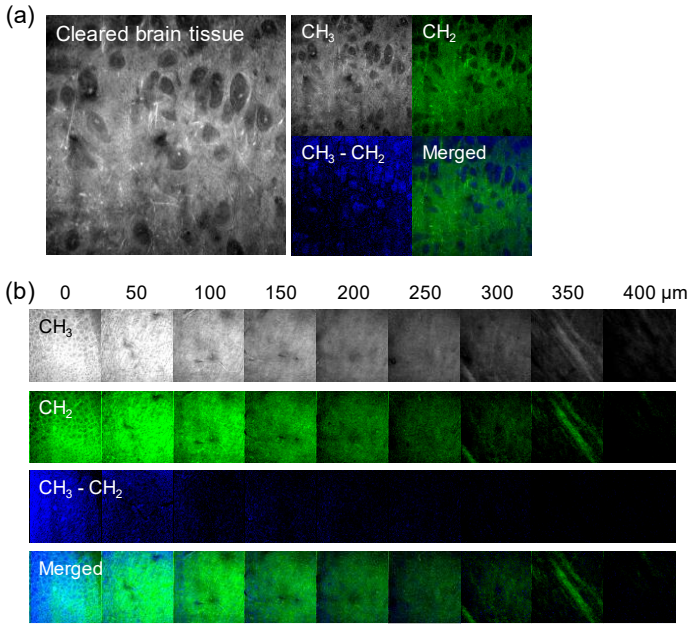


**Fig 5. Two-color SRS imaging of cleared tissue toward 3D histopathology.** (a) Left: maximum intensity projection image projected from a hyperspectral SRS image of a brain tissue slice cleared with ClearT method with 5% Triton X-100. Right: single frame SRS images at 2930 $cm^{-1}$ ($CH_3$), 2850 $cm^{-1}$ ($CH_2$), subtracted image ($CH_3$ – $CH_2$), and composite image of ($CH_3$ – $CH_2$) and ($CH_2$). (b) $CH_3$, $CH_2$, $CH_3$ – $CH_2$, and composite images of cleared brain slice at different depth.

To test whether this method works for cleared tissues, we firstly applied hyperspectral SRS imaging in the region from ~2800 $cm^{-1}$ to ~3050 $cm^{-1}$ to cleared brain tissue slice (**Movie 11**). SRS images at 2850 $cm^{-1}$ ($CH_3$) and 2930 $cm^{-1}$ ($CH_2$) show clear contrast between cells and background, because of much lower signal from clearing solution at these frequencies (**Fig. 5A**). Subtracting $CH_2$ image from $CH_3$ images results in an image with minimal background signal and highlighted nucleus areas. Composite of $CH_2$ image with the $CH_3 - CH_2$ image shows much improved contrast of nucleus and cytoplasm, generating a histology-like image with nucleus and cytoplasm highlighted in two pseudo colors (**Fig. 5A**). Using a lab-built LabView program, we acquired SRS images at two Raman shifts at different depths with a step interval of 1 μm. A three-dimensional histological image was obtained (**Fig. 5B, Movie 12**). These data collectively demonstrated ClearT based tissue clearing method is a useful technique to improve SRS imaging depth for rapid and accurate 3D histopathology.

## 4. Discussion and outlooks

There have been numerous efforts attempting to modernize the centuries-old 2D tissue slide based histopathology toward 3D histopathology. However, it has not been successful in revolutionizing the conventional histopathology framework. Most techniques are being developed to improve the imaging speed and depth, but still relies on staining with dyes. One inevitable limitation of staining is the slow diffusion speed (e.g., days) of dyes into bulk tissues over 1 mm in size. The time spent for histopathology is not reduced even with much faster imaging speed. Moreover, labeling efficiency varies with depth due to the gradient concentration of dyes through diffusion.

Label-free SRS histopathology avoids the need for dye staining by detecting intrinsic chemical bond vibrations. Chemical selectivity offers SRS microscopy the capability to visualize the tissue structure and cell morphology and provide histology-like contrast, which reduces the barriers that preventing pathologists adopting new techniques. Coupling tissue clearance, SRS imaging depth is improved to 500 μm, ~10-fold increase compared to tissues without clearance, allowing imaging of 1 mm thick tissue slices each time. Clearing of 1 mm thick slices only takes ~30 min, which is much faster than commonly used clearing method in fluorescence imaging, such as CUBIC or CLARITY [26], not even to say the time saved from staining. It becomes feasible to image the whole volume of a cm-size tissue block by sectioning it into a few 1 mm thick slices, instead of thousands of 5 μm thin slices. It will save tremendous time and efforts in registering individual slices and reconstructing them into 3D images, and minimize image distortion caused by loss of individual slices or variation in staining intensity of individual slices. Therefore, 3D SRS histopathology holds the promise to improve the accuracy and efficiency of clinical pathological diagnosis.

Besides histopathology, 3D SRS microscopy is a powerful tool in deciphering the cell-to-cell heterogeneity in complex tissue environment. For example, cancer tissues have long been known to exhibit intra-tumor heterogeneity [31, 32]. There is an urgent demand for single-cell analysis tools to reveal the morphological, genomic and metabolic information of individual cells. SRS microscopy is capable to reveal the morphological and metabolic information at single cell resolution. Brain tissues, as another example, have irregular organization and long-extending neuron cells. Elucidating the neural connection network relies on imaging with single-cell resolution in their 3D context. 3D SRS imaging has the potential to profile large number of cells in tissues in their native organization at single cell level.

In this study, we find ClearT solution can clear the tissues much faster (~30 min) than other small molecule aqueous solution based methods, which usually take days. The key molecule in ClearT solution is formamide. Compared to urea or other sugar molecules, such as sucrose or fructose, the molecular size of formamide is smaller and it is miscible with water. Therefore, it could diffuse deeper and faster than urea or sucrose. With our current imaging set up, the maximal depth we can achieve with discernable image quality is ~500 μm. The penetration depth could be further improved with higher excitation power, which is limited by the laser

source in our current set up. Using an objective with higher N.A. and long working distance (> 1 mm) could further improve the focus of light in deep tissue and eventually increase imaging depth. As SRS microscopy uses two laser beams (pump beam at 798 nm and Stokes beam at 1040 nm), chromatic aberrations between two beams might increase with depth. Through adaptive optics to correct the aberrations, one can potentially improve the spatial overlap between two beams at deep tissue level and consequently increase the imaging depth further.


## Funding

This work is supported by NIH R33CA223581 and NSF CHE1807106 to JXC.

## Acknowledgements

The authors acknowledge Dr. Chien-Sheng Liao for initial system setup and optimization.


## Disclosures

The authors declare that there are no conflicts of interest related to this article.

## References


1. Provenzano, E., et al., "Standardization of pathologic evaluation and reporting of postneoadjuvant specimens in clinical trials of breast cancer: recommendations from an international working group," Mod. Pathol. **28**, 1185 (2015).
2. Roberts, N., et al., "Toward Routine Use of 3D Histopathology as a Research Tool," Am. J. Pathol. **180**(5), 1835-1842 (2012).
3. Nolan, R.M., et al., "Intraoperative optical coherence tomography for assessing human lymph nodes for metastatic cancer," BMC Cancer **16**(1), 144 (2016).
4. Nguyen, F.T., et al., "Optical Coherence Tomography: The Intraoperative Assessment of Lymph Nodes in Breast Cancer," IEEE Eng. Med. Biol. Mag. **29**(2), 63-70 (2010).
5. Pilling, M. and P. Gardner, "Fundamental developments in infrared spectroscopic imaging for biomedical applications," Chem. Soc. Rev. **45**(7), 1935-1957 (2016).
6. Petibois, C. and G. Déléris, "Chemical mapping of tumor progression by FT-IR imaging: towards molecular histopathology," Trends Biotechnol. **24**(10), 455-462 (2006).
7. Fernandez, D.C., R. Bhargava, S.M. Hewitt, and I.W. Levin, "Infrared spectroscopic imaging for histopathologic recognition," Nat. Biotechnol. **23**, 469 (2005).
8. Tiwari, S., et al., "Towards Translation of Discrete Frequency Infrared Spectroscopic Imaging for Digital Histopathology of Clinical Biopsy Samples," Anal. Chem. **88**(20), 10183-10190 (2016).
9. Andrew Chan, K.L. and S.G. Kazarian, "Attenuated total reflection Fourier-transform infrared (ATR-FTIR) imaging of tissues and live cells," Chem. Soc. Rev. **45**(7), 1850-1864 (2016).
10. Wong, T.T.W., et al., "Fast label-free multilayered histology-like imaging of human breast cancer by photoacoustic microscopy," Sci. Adv. **3**(5), e1602168 (2017).
11. Fereidouni, F., et al., "Microscopy with ultraviolet surface excitation for rapid slide-free histology," Nat. Biomed. Eng. **1**(12), 957-966 (2017).
12. Glaser, A.K., et al., "Light-sheet microscopy for slide-free non-destructive pathology of large clinical specimens," Nat. Biomed. Eng. **1**, 0084 (2017).
13. Balu, M., G. Lentsch, D.Z. Korta, K. König, K.M. Kelly, B.J. Tromberg, and C.B. Zachary, "In vivo multiphoton-microscopy of picosecond-laser-induced optical breakdown in human skin," Lasers Surg. Med. **49**(6), 555-562 (2017).
14. Balu, M., H. Mikami, J. Hou, E.O. Potma, and B.J. Tromberg, "Rapid mesoscale multiphoton microscopy of human skin," Biomed. Opt. Express **7**(11), 4375-4387 (2016).
15. Popp, J. *Optical biopsies using multimodal imaging - chances and limitations*. in *Biophotonics Congress: Biomedical Optics Congress 2018 (Microscopy/Translational/Brain/OTS)*. 2018. Hollywood, Florida: Optical Society of America.
16. Bocklitz, T.W., et al., "Pseudo-HE images derived from CARS/TPEF/SHG multimodal imaging in combination with Raman-spectroscopy as a pathological screening tool," BMC Cancer **16**, 534-534 (2016).
17. Sun, Y., et al., "Intraoperative visualization of the tumor microenvironment and quantification of extracellular vesicles by label-free nonlinear imaging," Sci. Adv. **4**(12), eaau5603 (2018).
18. Cheng, J.-X. and X.S. Xie, "Vibrational spectroscopic imaging of living systems: An emerging platform for biology and medicine," Science **350**(6264), 1054 (2015).
19. Lu, F.-K., et al., "Label-Free Neurosurgical Pathology with Stimulated Raman Imaging," Cancer Res. **76**(12), 3451 (2016).
20. Ji, M., et al., "Detection of human brain tumor infiltration with quantitative stimulated Raman scattering microscopy," Sci. Transl. Med. **7**(309), 309ra163 (2015).

21. Ji, M., et al., "Rapid, Label-Free Detection of Brain Tumors with Stimulated Raman Scattering Microscopy," Sci. Transl. Med. **5**(201), 201ra119 (2013).
22. Orringer, D.A., et al., "Rapid intraoperative histology of unprocessed surgical specimens via fibre-laser-based stimulated Raman scattering microscopy," Nat. Biomed. Eng. **1**, 0027 (2017).
23. Chen, X., C. Zhang, P. Lin, K.-C. Huang, J. Liang, J. Tian, and J.-X. Cheng, "Volumetric chemical imaging by stimulated Raman projection microscopy and tomography," Nat. Commun. **8**, 15117 (2017).
24. Wei, M., et al., "Volumetric chemical imaging by clearing-enhanced stimulated Raman scattering microscopy," Proc. Natl. Acad. Sci. U.S.A. **116**(14), 6608 (2019).
25. Liu, B., H.J. Lee, D. Zhang, C.-S. Liao, N. Ji, Y. Xia, and J.-X. Cheng, "Label-free spectroscopic detection of membrane potential using stimulated Raman scattering," Appl. Phys. Lett. **106**(17), 173704 (2015).
26. Richardson, D.S. and J.W. Lichtman, "Clarifying Tissue Clearing," Cell **162**(2), 246-257 (2015).
27. Tsai, P.S., et al., "Correlations of Neuronal and Microvascular Densities in Murine Cortex Revealed by Direct Counting and Colocalization of Nuclei and Vessels," J. Neurosci. **29**(46), 14553 (2009).
28. Hama, H., et al., "Scale: a chemical approach for fluorescence imaging and reconstruction of transparent mouse brain," Nat. Neurosci. **14**, 1481 (2011).
29. Kuwajima, T., A.A. Sitko, P. Bhansali, C. Jurgens, W. Guido, and C. Mason, "ClearT: a detergent- and solvent-free clearing method for neuronal and non-neuronal tissue," Development **140**(6), 1364-8 (2013).
30. Fu, D. and X.S. Xie, "Reliable Cell Segmentation Based on Spectral Phasor Analysis of Hyperspectral Stimulated Raman Scattering Imaging Data," Anal. Chem. **86**(9), 4115-4119 (2014).
31. Lawson, D.A., K. Kessenbrock, R.T. Davis, N. Pervolarakis, and Z. Werb, "Tumour heterogeneity and metastasis at single-cell resolution," Nat. Cell Biol. **20**(12), 1349-1360 (2018).
32. Dagogo-Jack, I. and A.T. Shaw, "Tumour heterogeneity and resistance to cancer therapies," Nat. Rev. Clin. Oncol. **15**, 81 (2017).